Polymer 50 (2009) 2001–2009

Contents lists available at ScienceDirect

Polymer

journal homepage: www.elsevier.com/locate/polymer

Synthesis of terpyridine-functionalized poly(phenylenevinylene)s: The role of *meta*-phenylene linkage on the Cu^{2+} and Zn^{2+} chemosensors

Victor Banjoko [a,b], Yongqian Xu [a], Eric Mintz [b], Yi Pang [a,*]

[a] Department of Chemistry, Maurice Morton Institute of Polymer Science, The University of Akron, Akron, OH 44325, United States
[b] Department of Chemistry, Clark Atlanta University, Atlanta, GA 30314, United States

ARTICLE INFO

Article history:
Received 22 January 2009
Received in revised form
25 February 2009
Accepted 28 February 2009
Available online 11 March 2009

Keywords:
Fluorescence
Sensors
Conjugated polymers

ABSTRACT

A *meta*-phenylene-containing poly(phenylenevinylene) (PPV) with pendant terdentate terpyridine ligand **2b** was synthesized and its fluorescence properties were compared with its isomeric PPV. The *meta*-phenylene bridge interrupts the resonance connection between the PPV backbone and the metal-chelation sites, while jointing the structurally defined chromophores together. The fluorescence of the polymer, with emission $\lambda_{em} = 460$ nm and $\phi_{fl} \approx 0.45$, is found to be selectively quenched by Cu^{2+} ion with interference from Co^{2+} and Ni^{2+} ions. The nature of the quenching process in **2b** is probed by using Stern–Volmer analysis, revealing that the quenching results from both dynamic collision and metal chelation. Addition of Zn^{2+} and Cd^{2+} ions only induces partial fluorescence quenching, accompanied with a broad new emission band occurring at ~560 nm. With the aid of a model compound study, the new emission band at 560 nm is attributed to the complex formation with terpyridine to Zn ratio of 1:1. The study finds that the polymer has the potential for Cu^{2+} and Zn^{2+} sensors.

1. Introduction

Significant interest exists in recognizing the d-block metals, such as zinc and copper, which play an increasing role in neurobiology [1]. Many d-block metal ions are also a cause of environmental and public health concern as they are in the EPA's "priority pollutants list" [2,3]. These metal ions include chromium(III), Cobalt(II), Copper(I), zinc(II) Silver(I), mercury(II), cadmium(II). Lead(II), and nickel(II). The development of sensor molecules, which can selectively detect heavy metal ions, remains to be an important task for the detection and treatment of environmental contamination [4–7]. In the past two decades, fluorescence chemosensors [4,8] have received increasing attention, due to their high sensitivity of detection (down to the single molecule) and unique "on–off" switchability. Fluorescent chemosensors are typically consisting of two parts: a metal-chelating unit to selectively recognize the ion, and a fluorosphore to translate the metal-binding event to useful signal response. The effective optical signal response depends on the specific photophysical mechanism involved [9]. The field of chemical sensing continues to flourish with the discovery of novel materials, which combines new metal-binding and signal transducer mechanisms to achieve improved analyte recognition.

One of the most commonly used *N*-heterocyclic ligands is 2,2′:6′,2″-terpyridine (abbreviated as tpy), which binds with metals as a terdentate ligand [10]. Its unique cation-binding ability provides an effective building block in the assembly of various useful materials [11], generating both linear [12–14] and cyclic [15] molecular frames. For example, the terpyridine–Ru(III) complexes are efficient dye-sensitizers for solar energy conversion [16], while the terpyridine–Zn(II) complexes exhibit electroluminescence [12,13]. The assembly of these useful materials is based on the large binding constants between the tpy ligand and various metal ions.

π-Conjugated polymers have emerged as one of the most important classes of sensor materials [17], since their backbone readily transforms a chemical event into an easily measured electrical or optical signal. One of the attractive features is that the conjugated polymer backbones can transport electronic excited states. Under photon irradiation, the sensor molecule is sent to excited states, and the resulting exciton can rapidly migrate between isoenergetic sites along the conjugated polymer backbone to a low energy acceptor site. This exciton mobility within conjugated polymers forms a sequence of optical events, which can serve as an optical signal amplifier and produce signal gain in response to interactions with analytes. An efficient fluorescent quenching mechanism can be achieved with low quencher concentration because bonding at a single receptor site can result in efficient

* Corresponding author.
E-mail address: yp5@uakron.edu (Y. Pang).

0032-3861/$ – see front matter © 2009 Elsevier Ltd. All rights reserved.
doi:10.1016/j.polymer.2009.02.045

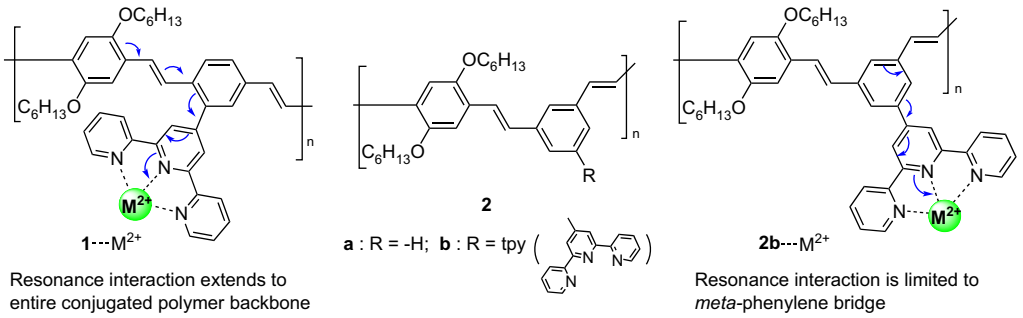

Scheme 1. Structures of polymers **1** and **2**, and their respective metal complexes.

quenching of multiple emitting units along the polymer backbone [18], thereby amplifying the signal output.

Poly(1,4-phenylene vinylene) (PPV) derivatives are highly luminescent materials for light-emitting diodes (LEDs) [19]. By attaching a tpy unit on the PPV backbone, Kimura et al. [20]. have shown that the fluorescence of the polymer (**1**) was quenched completely by Fe^{2+}, Fe^{3+}, Ni^{2+}, Cu^{2+}, Cr^{2+}, Mn^{2+}, and Co^{2+}. In addition, the Zn^{2+} cation induces only partially quenching of the fluorescence, and causes the emission peak red-shifted from 524 nm to 563 nm. The indiscriminate fluorescence quenching, observed from the terpyridine-functionalized PPV, indicates strong coupling between the metal-binding tpy and PPV polymer backbone. It should be noted that the tpy in **1** is placed at *ortho* position relative to one of the two vinylene bonds, which allows the electronic resonance interaction between the tpy and conjugated polymer backbone. As seen from the metal complex **1**$\cdots M^{2+}$, the metal-binding-induced resonance interaction is easily extended to the entire conjugated backbone (Scheme 1).

Recent studies have also shown that the poly[(*m*-phenylenevinylene)-*alt*-(*p*-phenylenevinylene)] (P*m*PV*p*PV) derivative **2a** is green-emitting with high photoluminescence efficiency [21,22]. Alternate occurrence of *meta*-phenylene units along the P*m*PV*p*PV chain effectively breaks the conjugated backbone into a sequence of well-defined chromophores (or isoenergetic molecular fragments). For chemosensor applications, it would be interesting to examine the P*m*PV*p*PV derivative **2b**, in which the tpy is placed at the *meta* position relative to both vinylene bonds along the chain. As shown in the metal complex **2b**$\cdots M^{2+}$, the resonance interaction from the tpy center is only transmitted up to the *meta*-phenylene bridge. The molecular design of **2b**, therefore, limits the resonance interaction between the tpy and polymer backbone. Reasoning that such weakened electronic connection in **2b** could be used to attenuate the signal transfer between the tpy sensing site and fluorescent polymer backbone, we decide to synthesize polymer **2b** and to examine its selectivity in metal ion binding. A section of polymer **2b** is shown by the molecular fragment **6**, where two identical chromophores are intimately fused together via sharing a common *meta*-phenylene unit. This unique structural feature allows one tpy unit to simultaneously affect the two adjacent chromophores along the polymer backbone, thereby improving the optical signal response.

2. Results and discussion

2.1. Polymer synthesis and characterization

Terpyridine **3** was obtained by the reaction of 3,5-dimethylbenzaldehyde with 2 equiv of 2-acetylpyridine (Scheme 2). The desirable monomer, bis(triphenylphosphonium bromide) **5**, was prepared by bromination of **3** using a similar literature procedure

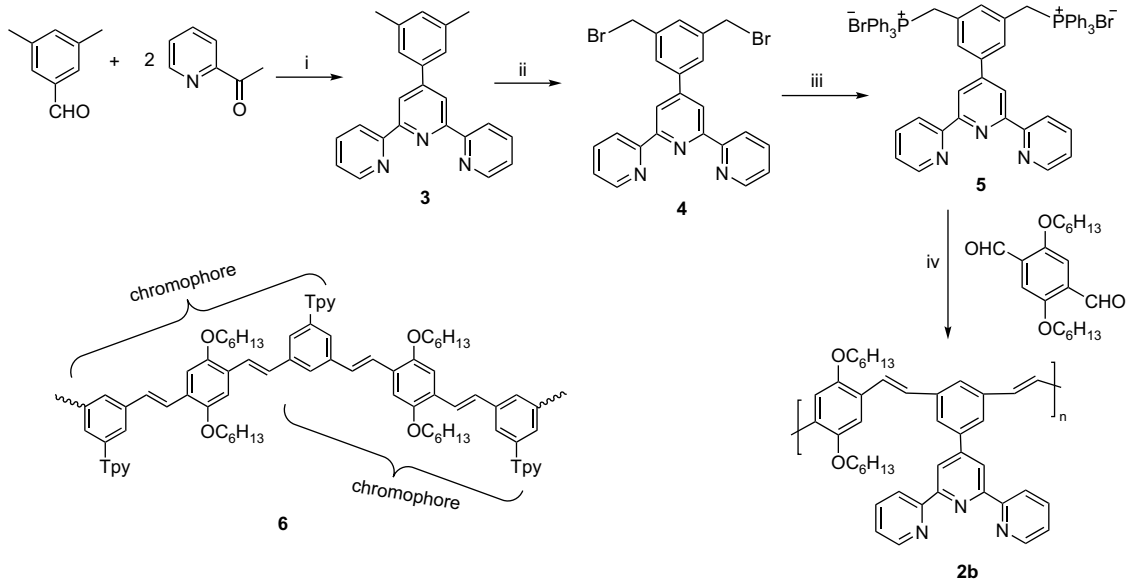

Scheme 2. Polymer synthesis. Reagents and conditions: (i) KOH, NH_4OH, EtOH, room temperature or reflux, 24 h, 30%; (ii) NBS, BPO, CCl_4, reflux, 3 h, 30%, (iii) PPh_3, EtOH, 15 h, 30%; (iv) NaOEt, THF, 24 h, 70%; I_2.

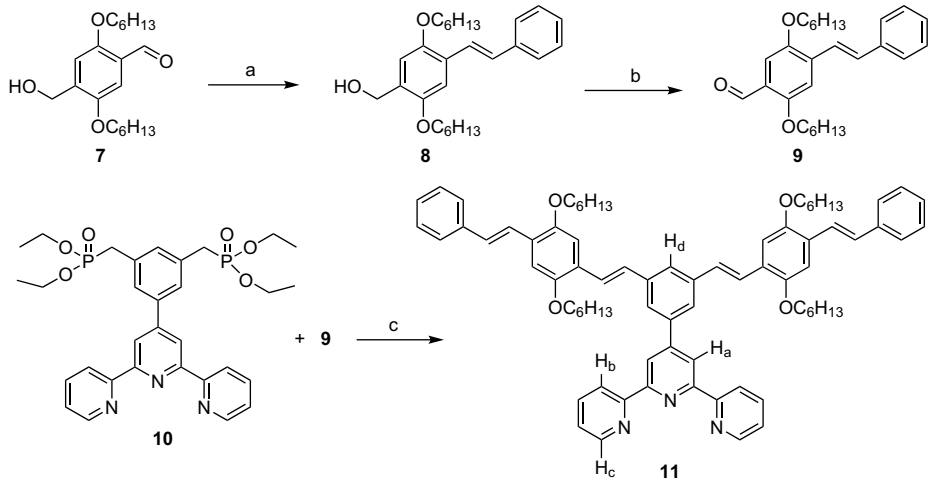

Scheme 3. Synthesis of model compound. Reagents and conditions: (a) benzyltriphenylphosphonium bromide, NaH, THF, reflux; (b) pyridinium chlorochromate, CH_2Cl_2, room temperature; (c) potassium *tert*-butoxide, THF.

[23], followed by reaction with triphenylphosphine. Wittig condensation [24,21] followed by iodine-catalyzed isomerization gave **2** as an orange solid, which had an average molecular weight $M_w = 6750$ against a polystyrene standard by GPC.

To assist the structural and property evaluation, the model compound **11** was synthesized similarly (Scheme 3). Wittig reaction between benzyltriphenylphosphonium bromide and monoaldehyde **7** provided compound **8**, which was followed by oxidation to give desirable aldehyde **9**. Condensation of phosphonate **10** with aldehyde **9** led to the model compound in which all C=C bonds are in *trans*-configuration. The compound **11** was purified on column chromatography to remove the *cis*-CH=CH-containing fraction.

^{1}H NMR spectra of **2b** and **11** were matched well (Fig. 1), supporting the proposed polymer structure for the former. The resonance signal at 4.1 ppm was attributed to $-OCH_2-$, which is known to be sensitive to the vinyl bond geometry [21]. Absence of $-OCH_2-$ signal at ~3.5 ppm further confirmed that all the C=C bonds were in *trans*-configuration. The ^{1}H NMR spectrum of **11** revealed the terpyridine proton H_a as a singlet at ~8.8 ppm, and H_b and H_c as the expected doublets between 8.7 and 8.8 ppm. The proton H_d was observed at 7.8 ppm. These characteristic peaks were all visible in the polymer spectrum.

2.2. Absorption spectra and metal ion titration

The UV–vis spectrum of **2b** showed strong absorption bands at 327 and 401 nm (Fig. 2), which were very similar to that of **2a** without tpy substitution ($\lambda_{max} = 328$, 406 nm) [21]. The band at 401 nm was attributed to the π–π transition of the conjugated backbone, and tpy substitution posed negligible steric influence on the P*m*PV*p*PV backbone. The addition of Fe(II) ion to the polymer solution of **2b** resulted in a slight decrease in absorbance without notable shift in peak position. This is in contrast to **1** where addition of Fe(II) ion caused a gradual blue shift (about 24 nm) [20] for the π–π absorption band of the PPV backbone. The solution of **2** became purple upon addition of Fe(II), revealing a new peak at 575 nm which is attributed to the metal-to-ligand charge transfer (MLCT) band. The maximum absorbance at 575 nm was reached at an approximate ratio of tpy:Fe(II) ≈ 2:1 (shown in the inset of

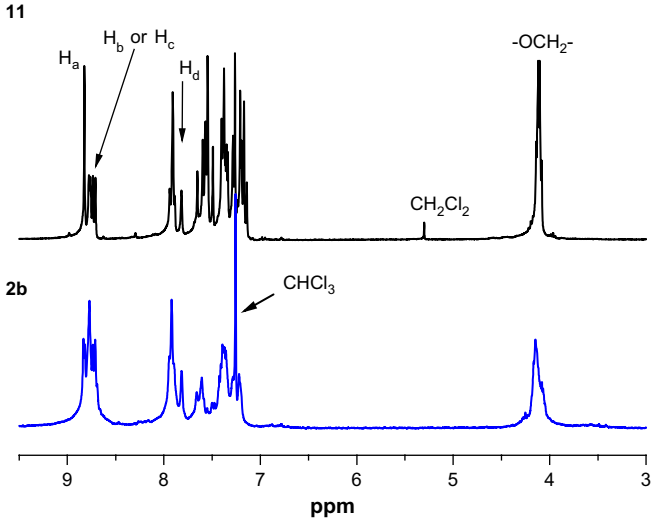

Fig. 1. ^{1}H NMR spectra of polymer **2b** (bottom) and model compound **11** (top) in $CDCl_3$. The solvent residue peaks are indicated as labeled. The alkyl region was omitted for clarity.

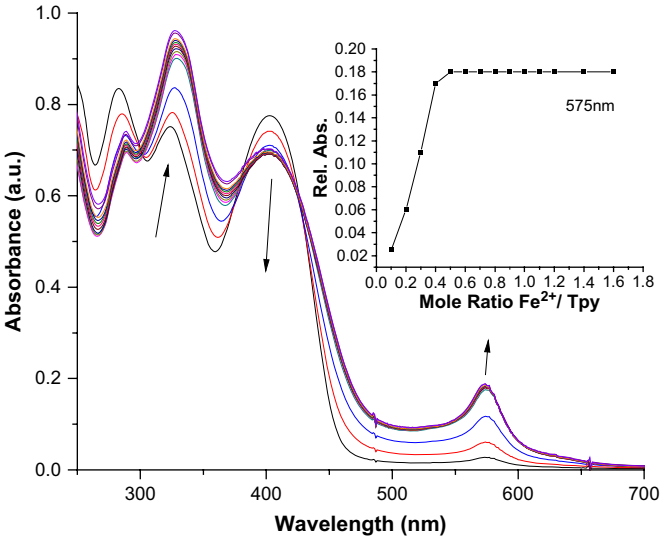

Fig. 2. Effect of Fe^{2+} concentration on the absorption spectra of **2b** (1.0×10^{-5} M corresponding to terpyridyl segments) in $CHCl_3$–MeOH:[Fe^{2+}]/tpy ratio = 0.1, 0.2, 0.5, 1.0, 1.2, 1.4, 1.6. Arrows indicate the direction of spectral changes. The inset shows the relationship between Fe^{2+} concentration and the absorbance at 570 nm.

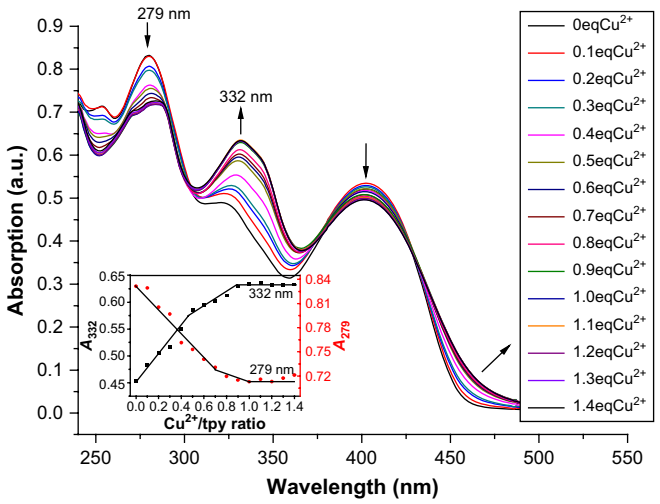

Fig. 3. Effect of Cu^{2+} on the absorption spectra of **2b** (1.0×10^{-5} M corresponding to terpyridyl segments) in $CHCl_3$–MeOH. Arrows indicate the direction of spectral changes. The inset shows the influence of the molar ratio of Cu^{2+} to terpyridyl groups on the absorbance at 332 nm (square) and 279 nm (circle).

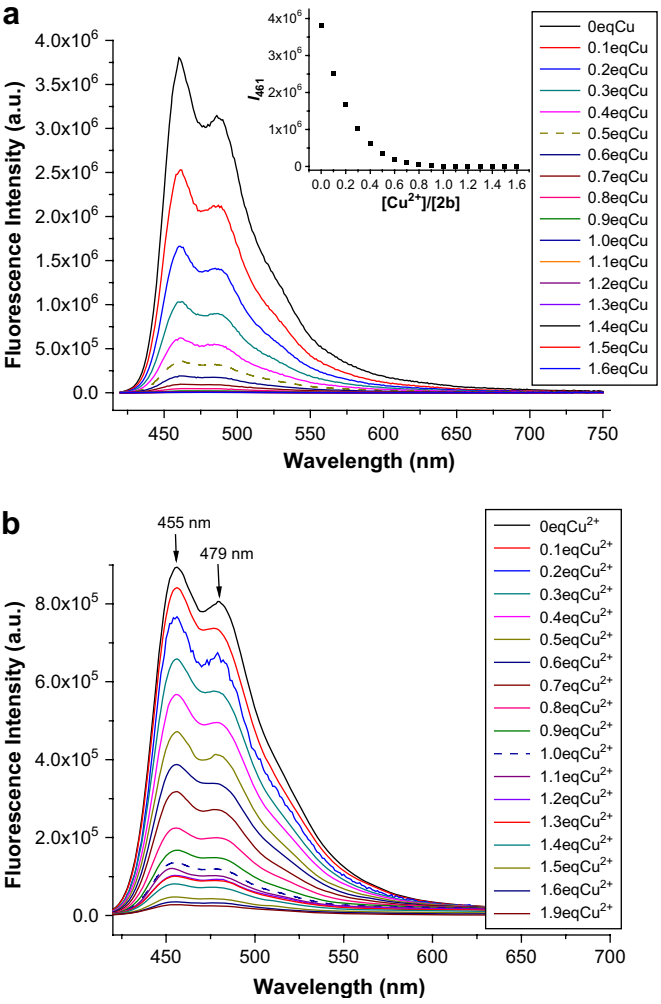

Fig. 4. The fluorescence emission spectra of **2b** (10^{-6} M, top) and **11** (10^{-6} M, bottom) in the presence of different amounts of Cu(II) in $CHCl_3$/MeOH (9:1, v/v).

Fig. 2). The MLCT band of **2** was at a longer wavelength than that of **1** (MLCT band at 568 nm) [20], suggesting that the tpy in the former had a slightly lower π^*-energy level than that in the latter.

Effect of Cu^{2+} ion on the absorption of **2b** revealed the similar trend, as the absorbance of the π–π band at 401 nm decreased slightly with increasing metal ion concentration (Fig. 3). Different from the tpy–Fe(II) complexation, the MLCT band was observed as a broad featureless tail at the absorption edge (or spectral onset) at ~460 nm. The same characteristics were also observed for the other metal ions tested, including Ni^{2+}, Cd^{2+}, Hg^{2+}, Cr^{6+}, Co^{2+}, and Ag^{2+}. By using the absorption peak at 323 or 279 nm, the ratio of tpy:Cu(II) was estimated to be about 1:1. It should be noted that copper(II) typically favors the coordination number of 4 and 5 (less than 6) [25], although tpy–Cu(II) complexes of both 1:1 ratio [26] and 2:1 ratio [27] have been reported. The absorption of **11** in $CHCl_3$–MeOH (9:1 by volume) gave the similar profile as **2b**, revealing absorption bands at $\lambda_{max} = 328$ and 398 nm. Titration of **11** with Cu^{2+} also showed that the maximum absorbance response occurred when the ratio of **11**:Cu(II) reached 1:1, in consistency with the finding from the polymer **2b**.

2.3. Fluorescence properties

Fluorescence of **2b** (Fig. 4) exhibited emission peaks at 460 and 488 nm, which were attributed to the lowest energy π–π^* excited state on the PPV backbone. The fluorescence quantum yield of **2b** in CH_3Cl_3/CH_3OH (9:1 ratio) was measured to be $\phi_{fl} = 0.45$, by using quinine sulfate standard [28]. Addition of Cu^{2+} in the CH_3Cl_3/CH_3OH resulted in significant fluorescence quenching of **2b** (Fig. 4), which was further confirmed from the titration of the model compound **11**. Similar fluorescence quenching, but in less degree, was also observed from **2b** upon addition of Co^{2+}, Ni^{2+}, or Hg^{2+} cations. Screening of different metal ions showed that the polymer **2b** was much more sensitive to quenching by Cu^{2+} cation (Fig. 5), with sensitivity in the order of $Cu^{2+} > Co^{2+} > Ni^{2+} > Hg^{2+} > Zn^{2+} > Cd^{2+}$. In addition, the Cr^{3+}, Fe^{3+}, and Mn^{2+} ions did not quench the fluorescence. The spectrum of fluorescence response to different cations was visible (Fig. 6), as **2b** remained to be weakly fluorescent in the presence of Hg^{2+} cation (in comparison with Cu^{2+}, Co^{2+} and Ni^{2+}). The observation from the fluorescence of **2b** appeared to be in contrast to that of its isomer **1**, as the latter

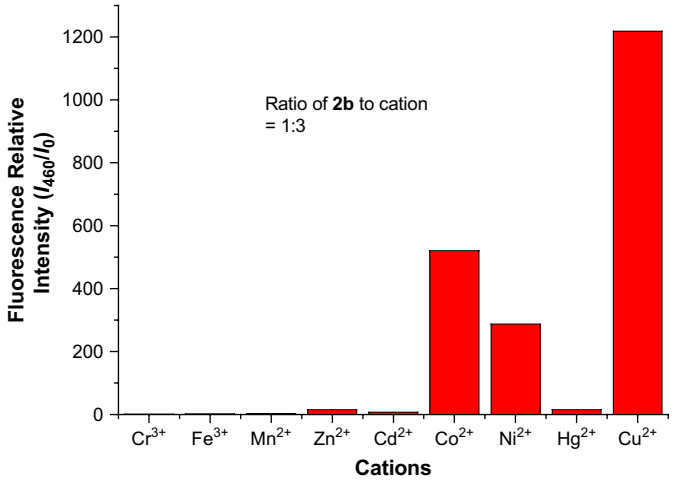

Fig. 5. Emission quenching profile for **2b** (1.0×10^{-5}) by different metal ions (3 equiv) in $CHCl_3$/MeOH (ratio = 9:1) solution. Excitation wavelength was 420 nm and the emission intensities were calculated at their respective peak λ_{max}. The fluorescence intensity at 460 nm in the presence (I_{460}) and absence (I_0) of metal ions was used to calculate the ratio I_{460}/I_0.

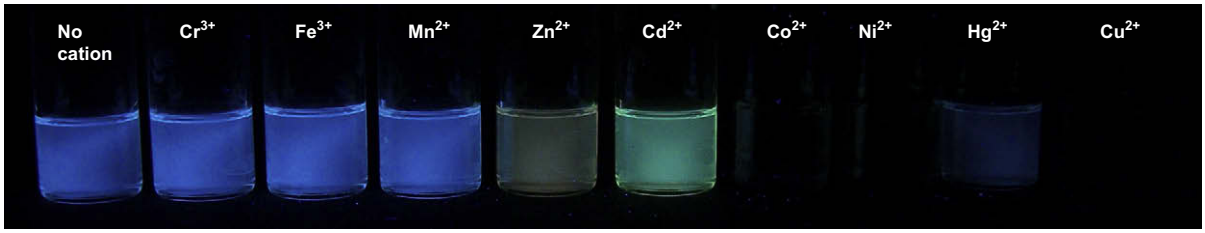

Fig. 6. Fluorescence images of **2b** (1.0×10^{-5}) in the presence of different cations (3 equiv) in $CHCl_3$/MeOH (ratio = 9:1) solution.

polymer was quenched completely by Cu^{2+}, Fe^{3+}, Ni^{2+}, Cr^{2+}, Co^{2+} and Mn^{2+} cations, and partially by Zn^{2+} cation [20]. A possible rational is that the *meta*-positioned terpyridyl group in **2** does not have resonance interaction with the chromophore along the polymer backbone. This structural feature weakens the electronic connection between the chromophore (polymer backbone) and the metal-chelation site, thereby attenuating the fluorescence quenching by metal cations to allow the observed selectivity.

The fluorescence quenching behavior can be attributed to many factors, including quenching mechanisms, nature of metal ions, and metal–ligand binding strength. The observed trend appears to be in consistent with the general stability constants for metal complexes, known as Irving–Williams series ($Cu^{2+} > Ni^{2+} > Co^{2+} > Fe^{2+} > Mn^{2+} > Mg^{2+}$) [25]. The stronger quenching effects from Cu^{2+}, Co^{2+}, and Ni^{2+} cations could, therefore, be due a combination of their strong binding with tpy ligand [29] and their paramagnetic property. The heavy atom effect [30], however, is responsible for the fluorescence quenching from the Hg^{2+} cation, as the metal ion has a d- [10] electron configuration. Since the heavy atom effect operates via spin–orbital coupling, the interaction between the PPV backbone and Hg^{2+} site in **2b** appears to be affected by the decreased electronic connection.

2.4. Stern–Volmer analysis

The nature of the quenching process in **2b** was probed by Stern–Volmer analysis [30]. In the analysis, the relative fluorescence intensity (I_0/I) is plotted versus the concentration of quencher ions [Q], according to Equation (1). The slope of the line is equivalent to K_{sv}, which represents the rate of dynamic quenching.

$$\frac{I_0}{I} = 1 + K_{sv} \cdot [Q] \quad (1)$$

Dynamic quenching involves deactivation of the polymer exciton through collisions with quencher molecules or ions in solution. For a process of purely dynamic quenching, a linear line is expected, and the slope of the line gives K_{sv} constant. Presence of the terpyridine group along the polymer chain, however, allows a tight binding of the cation, which creates additional pathways for exciton relaxation and results in static quenching.

Stern–Volmer plot for quenching of **2b** and **11** by Cu^{2+} cation was constructed by using the steady-state fluorescence data (Fig. 7), exhibiting the nearly identical feature. At the relative low concentration of Cu^{2+}, the quenching was approximate linear, suggesting predominately dynamic quenching. It was possible that the cation was exchanged quickly at the different terpyridine binding sites, making the quenching process as a pseudo-dynamic one. When the Cu^{2+} concentration was 0.6×10^{-6} M and higher, however, the slope turned sharply up, indicating a stronger quenching process in play. This could be attributed to the strong cation binding to the terpyridine chelating groups, as less free terpyridine were available to participate in equilibrium with Cu^{2+} species. This led to static quenching and a positive deviation from the linear Stern–Volmer line, which was precedent in a tpy-containing π-conjugated polymer [31]. After 1 equiv Cu^{2+} cation was added (conc larger than 1.0×10^{-6} M), the slope of the Stern–Volmer plot turned to normal. It appeared that all the terpyridine chelating sites were occupied by the cations, which is consistent with the finding that the ratio of terpyridine to Cu^{2+} was 1:1 in the complex.

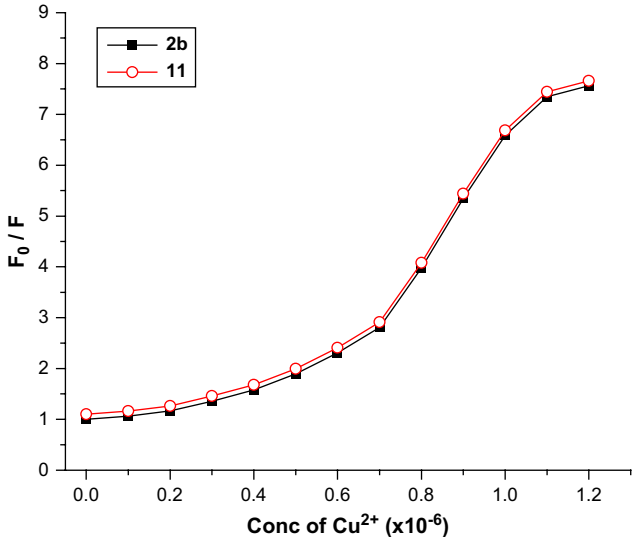

Fig. 7. Stern–Volmer plot for the quenching of **2b** and **11** (10^{-6} M) by Cu^{2+}. The curve for **11** is slightly offset from **2b** for comparison.

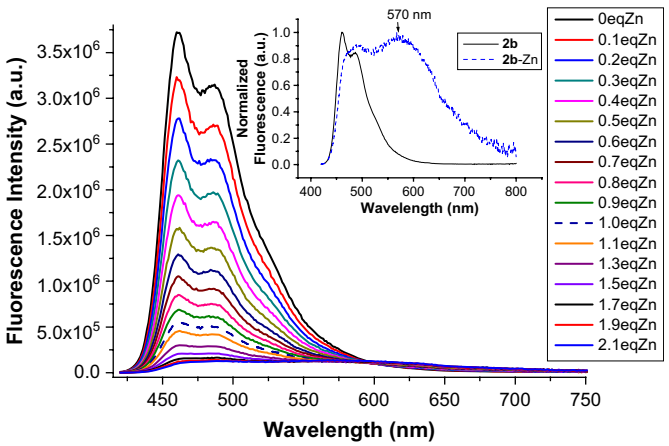

Fig. 8. Fluorescence response of **2b** (1×10^{-6} M) upon addition of $Zn(ClO_4)_2$ in $CHCl_3$/MeOH (9/1). The inset (normalized fluorescence) shows the influence of Zn^{2+} on the emission wavelength, revealing a new peak at ~570 nm.

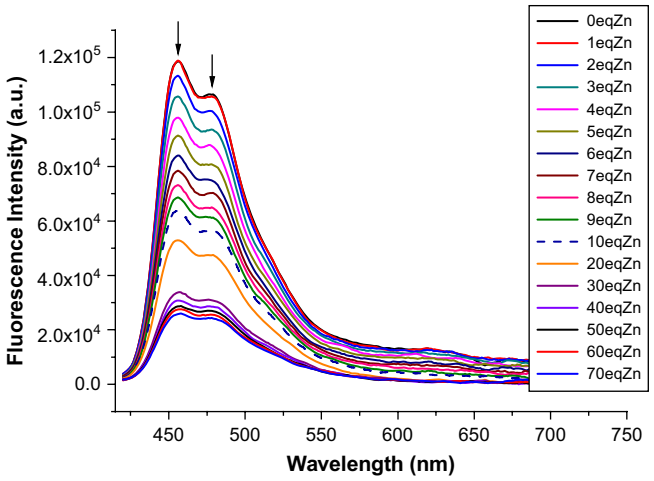

Fig. 9. Fluorescence response of **11** (1×10^{-6} M) upon addition of $Zn(ClO_4)_2$ in $CHCl_3$/MeOH(9/1).

2.5. Zinc–terpyridine complexes

Among the cations tested, the Zn^{2+} and Cd^{2+} cations exhibited notable impact on the emission color of **2b**, with the cadmium showing slightly less quenching effect (Figs. 5 and 6). When the Zn^{2+} cation was added to **2b** solution, the emission intensity at about 461 nm was notably decreased (Fig. 8), which accompanied with a broader but weaker band at ~570 nm for yellow emission. Addition of 1 equiv Zn^{2+} led to about 80% of the fluorescence quenching. The result was consistent with what observed from its isomer **1**, where the cation Zn^{2+} induces notable fluorescence quenching (by ~50%) and spectral red-shift (from 524 to 563 nm) [20]. The effect of zinc(II)-induced fluorescence quenching in **2b** was compared with the model compound **11**, where at least 10 equiv of Zn^{2+} was required to quench about 50% of the fluorescence signal (Fig. 9). The higher sensitivity to the zinc(II)-induced fluorescence quenching from the polymer **2b** could be related to the higher local concentration of tpy in the polymer solution, which would result in more effective zinc binding. Exciton migration along the polymer chain, which is absent in the model compound, is believed to play an important role in the observed fluorescence quenching, since the adjacent chromophores shared a common *meta*-phenylene bridge (as shown in fragment **6**).

Addition of $ZnCl_2$ to **2b** was assumed to form the complex **2b**–Zn, as the tpy and zinc(II) cation tend to form the complex in a 1:1 ratio [32]. To further confirm that the spectral red-shift ($\lambda_{em} \approx 575$ nm) and fluorescence quenching were due to the zinc–tpy complex formation, **2b** and **11** were reacted with 1 equiv of $ZnCl_2$ in a mixture of $CHCl_3$ and MeOH under reflux condition. Poor solubility of the obtained polymeric complex **2b**–Zn, however, hampered its purification and structural characterization by NMR. ^{1}H NMR of the complex **11**–Zn (Fig. 10) revealed that the resonance signals were broadened. The resonance signals between 8.7 and 8.8 ppm on the tpy of the free ligand **11** were split into two groups of signals (a proton at ~9 ppm, and two protons between 7.9 and 8.4 ppm) in the complex **11**–Zn as a result of metal binding. Complete disappearance of signals between 8.7 and 8.8 ppm, which were attributed to non-binding tpy group on the ligand **11** (Fig. 1), indicated that the reaction proceeded cleanly to afford **11**–Zn.

Attempt to detect **11**–Zn by mass spectrometry was not successful. The reaction of **11** with $Zn(OAc)_2$ in a mixture of $CHCl_3$/MeOH solvent, however, produced **11**–$Zn(OAc)_2$. Mass spectrum of the resulting solution observed $[\mathbf{11}\text{–}Zn(OAc)]^+$ at 1242.7 *m*/*z* as the major component, further supports the formation of **11**–Zn in which the tpy ligand binds to Zn^{2+} cation in a 1:1 ratio.

UV–vis absorption spectrum of **11** revealed λ_{max} at 324 and 399 nm (Fig. 11), which were essentially not changed upon formation of the **11**–Zn complex. The absorption edge at ~450 nm was slightly red-shifted for **11**–Zn, as a result of zinc binding [32], which is even more pronounced in **2b**–Zn complex. Since the absorption band at ~400 nm was attributed to the π–π transition of the conjugated backbone, the results indicated a stronger electronic coupling between the metal-binding site and the conjugated backbone in the polymer. The strong interaction between the PPV

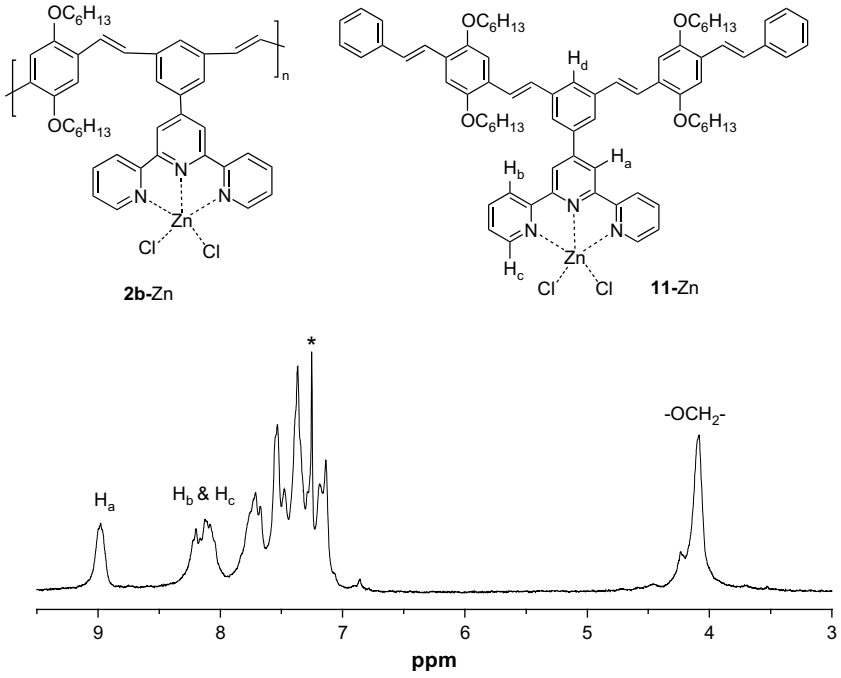

Fig. 10. ^{1}H NMR spectrum of complex **11**–Zn in $CDCl_3$. The starred signal at 7.25 ppm is attributed to $CHCl_3$ residue.

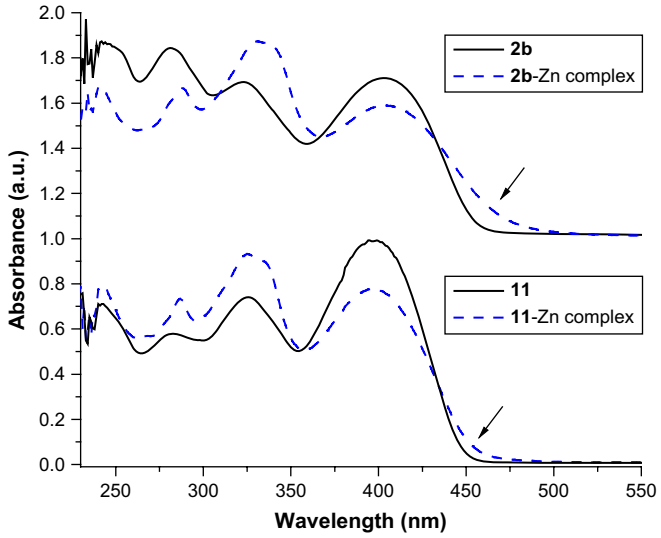

Fig. 11. UV–vis spectra of **2b** and **11** and their respective zinc complexes (1×10^{-5} M) in CH_3Cl. The arrows indicate the zinc chelation-induced change at the absorption edge.

and zinc-binding site contributed, at least in part, to the polymer's higher sensitivity in the zinc(II)-induced fluorescence quenching.

The emission spectrum of **11**–Zn significantly decreased the fluorescence intensity, accompanied with a large spectral shift (~100 nm) to give emission at 561 nm (Fig. 12). The diminished emission band at 455 nm in the complex indicated that the response of **11** to zinc(II)-induced fluorescence quenching was originated from zinc binding under the dilute condition. The emission of **11**–Zn complex displayed one shoulder at about 470 nm, which was basically insensitive to the temperature change and resolved into a pronounced band at −60 °C (inset in Fig. 12). The emission band at 470 nm was attributable to residual ligand **11**. In contrast, the major emission of **11**–Zn complex at 560 nm was shifted to ~620 nm, indicating that the emission of metal-chelation center was sensitive to the local environmental change. It should be pointed out that the emission profile of **11**–Zn resembled that of **2b**–Zn complex (inset in Fig. 8). The results support the assumption that the broad emission band at about 570 nm observed in the zinc titration of **2b** (Fig. 8) was due to the zinc(II) complex formation.

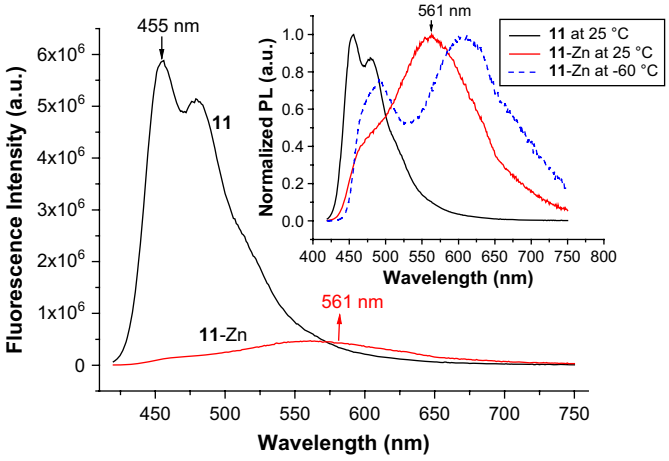

Fig. 12. Comparison of emission between **11** (10^{-6} M) and **11**–Zn (10^{-6} M) in CH_3Cl upon excitation at 400 nm. The inset is the normalized spectra showing the spectra of **11** and **11**–Zn at 25 °C (solid line), and **11**–Zn at −60 °C (broken line).

3. Experimental

3.1. Materials and general procedure

Triethylphosphite, benzyltriphenylphosphonium and zinc chloride were purchased from Aldrich, and NaH, pyridinium chlorochromate, potassium *tert*-butoxide were from Acros. Anhydrous THF solvent was freshly distilled over sodium, and other solvents were received from Acros or Fisher and were used without further purification. 4′-(3,5-Bis(bromomethyl)phenyl)-2,2′:6′,2″-terpyridine (**4**) was synthesized according to the literature procedure [23]. NMR spectra were collected on a Varian 300 Gemini spectrometer. UV–vis spectra were acquired on a Hewlett-Packard 8453 diode-array spectrometer. Fluorescence spectra were obtained on a HORIBA Jobin Yvon NanoLog spectrometer. The fluorescence quantum yield was obtained by using quinine sulfate as the standard ($\Phi = 0.53$ at 366 nm, 0.1 M H_2SO_4) [33]. Size exclusion chromatography (SEC) analysis was performed on a Waters 510 system equipped with three Waters styragel high resolution columns (a single porosity column HR1 100 Å, and two mixed-porosity columns HR4E and HR5E with 50, 500, 10^3, 10^4, 10^5, 10^6 Å), a Waters 410 differential refractometer, and a Wyatt Dawn EOS multiangle laser light-scattering (MALLS) detector. The experiments were carried out in THF at 35 °C at a flow rate of 1.0 ml/min. The results were analyzed by using Wyatt ASTRA v4 software.

3.2. Synthesis of monomer **5**

1-Terpyridyl-3,5-xylenebis(triphenylphosphonium bromide) was prepared by using a similar literature procedure [21]. ^{1}H NMR ($CDCl_3$): δ 8.91–9.01 (m, 2H, pyridine), 7.57–7.90 (m, 41H, pyridine and phenyl-H), 5.35 (d, $J = 15.5$ Hz, 4H, $CH_2P(Ph))_3$.

3.3. Synthesis of polymer **2b**

In an oven-dried 25 ml round-bottomed flask, monomers **5** (0.3 g, 0.3 mmol) and 2,5-bis(hexyloxy)benzene-1,4-dialdehyde (0.1 g, 0.3 mmol) were dissolved in a mixture of anhydrous EtOH (5 ml) and dry THF (5 ml). To the flask was added dropwise a solution of sodium ethoxide (NaOEt, 1 M, 0.8 ml) at room temperature. The reaction mixture was stirred for 24 h at room temperature, and the solvent was evaporated on a rotatory evaporator. The polymer was purified by dissolving in $CHCl_3$ followed by precipitation from methanol. This *cis*-CH=CH was converted to *trans*-CH=CH by refluxing the polymer in toluene with catalytic amount of iodine (I_2) [21]. In a typical procedure, 500 mg of the polymer was dissolved in 15 ml of toluene. To this solution was added a catalytic amount of iodine. The mixture was refluxed for a minimum of 4 h. The polymer was obtained as an orange solid (0.13 g, 70%) after precipitation from methanol. The molecular weight of the polymer was determined to be 6750 based on GPC analysis by using polystyrene as standard. ^{1}H NMR ($CDCl_3$, 300 MHz, δ ppm): 8.83 (br, 2H, pyridine), 8.77 (s, 2H, pyridine), 8.72 (d, $J = 6.0$ Hz, 2H, pyridine), 7.86–8.03 (br, 4H), 7.82 (s, 1H), 7.7–7.12 (Ar–H and vinyl proton), 4.16 (br, 4H, –OCH_2–), 1.92 (br, 4H, –CH_2–), 1.58 (br, 4H, –CH_2–), 1.34 (br, 8H, –CH_2–CH_2–), 0.84 (br, 6H, –CH_3). Anal. Calcd for $C_{43}H_{47}N_3O_2$: C, 81.23; H, 7.13; N, 6.61. Found: C, 80.48%; H, 7.11%; N, 6.61.

3.4. 2,5-Dihexyloxy-4-(hydroxylmethyl)benzaldehyde (**7**)

It was prepared using a modified procedure [34]. The product had the following spectral properties. ^{1}H NMR ($CDCl_3$, 300 MHz, δ ppm): 10.45 (s, 1H), 7.27 (s, 2H), 7.02 (s, 2H), 4.72 (d, $J = 6.0$ Hz,

2H), 4.02 (m, 4H), 2.37 (m, 1H), 1.81 (m, 4H), 1.45 (m, 4H), 1.34 (m, 8H), 0.91 (m, 6H). IR (KBr): 1655.56 cm^{-1}, 1613.58 cm^{-1}.

3.5. (*E*)-2,5-Bis(hexyloxy)-4-(styrylphenyl)hydroxymethylbenzene (**8**)

Sodium hydride (0.35 g, 5.94 mmol, 60% in mineral oil) was added to a suspension of benzyltriphenylphosphonium in dry THF (25 ml) under argon, and the reaction mixture was refluxed with stirring for 3 h. The appearance of orange color and the disappearance of the suspension of phosphonium salt indicated the yield formation. 2,5-Dihexyloxy-4-(hydroxylmethyl)benzaldehyde (**7**) (2.3 g, 5.94 mmol) was then added, and the resulting reaction mixture was heated to reflux for 40 h. After removing the solvents on a rotatory evaporator, the residue was purified on a silica column to afford a yellow oil (2.37 g, 97.1%). ^{1}H NMR ($CDCl_3$, 300 MHz, δ ppm): 7.56 (d, $J = 6.3$ Hz, 2H), 7.38 (dd, $J = 7.8$ Hz, $J = 6.3$ Hz, 2H), 7.29 (m, 2H), 7.11 (s, 1H), 6.90 (d, $J = 13.5$ Hz, 1H), 6.74 (m, 1H), 4.71 (s, 2H), 4.02 (m, 4H), 1.84 (m, 4H), 1.55 (m, 4H), 1.39 (m, 6H), 0.96 (m, 8H). ^{13}C NMR ($CDCl_3$, 75 MHz, δ ppm): 151.08, 138.18, 129.25, 129.00, 128.87, 128.37, 126.72, 125.80, 123.81, 113.85, 112.31, 109.30, 69.84, 69.42, 68.95, 68.89, 68.45, 62.08, 31.90, 29.35, 26.31, 26.19, 26.06, 22.87, 14.31.

3.6. (*E*)-2,5-Bis(hexyloxy)-4-(styrylphenyl)benzaldehyde (**9**)

Pyridinium chlorochromate (PCC) (1.85 g, 8.59 mmol) and dichloromethane (200 ml) were mixed into a 500 ml round bottom flask. (*E*)-2,5-Bis(hexyloxy)-4-(styrylphenyl)hydroxymethylbenzene (**8**) (2.35 g, 5.72 mmol) in dichloromethane (10 ml) was then added dropwise to the reaction mixture at room temperature. The solution color changed to dark and black solid precipitated. The reaction mixture was stirred for additional 3 h after addition. The crude product was purified on a silica column by using dichloromethane as eluent to give a yellow oil (1.5 g, 64.1%). ^{1}H NMR ($CDCl_3$, 300 MHz, δ ppm): 10.43 (s, 1H), 7.51 (dd, $J = 7.2$ Hz, $J = 10.2$ Hz, 2H), 7.35 (dd, $J = 5.7$ Hz, $J = 7.2$ Hz, 2H), 7.26 (m, 3H), 7.19 (s, 1H), 7.12 (s, 1H), 4.00 (m, 4H), 1.80 (m, 4H), 1.47 (m, 4H), 1.34 (m, 8H), 0.91 (m, 6H). ^{13}C NMR ($CDCl_3$, 75 MHz, δ ppm): 156.35, 155.36, 150.89, 137.45, 134.36, 132.37, 129.40, 128.95, 128.39, 127.08, 124.37, 123.06, 111.68, 110.64, 110.17, 69.32, 31.81, 29.44, 29.33, 29.23, 26.08, 26.02, 22.84, 14.26.

3.7. 4′-(3,5-Bis(diethylphosphonomethyl)phenyl)-2,2′:6′,2″-terpyridine (**10**)

A solution of 4′-(3,5-bis(bromomethyl)phenyl)-2,2′:6′,2″-terpyridine (**4**) (0.62 g, 1.25 mmol) and triethylphosphite (5 ml, 0.2 mol) in $CHCl_3$ (5 ml) was heated to reflux for 5 h. The solution was then cooled to room temperature, and chloroform and triethylphosphite were removed under reduced pressure. The product was obtained as a yellow oil (0.76 g) and was used for next step without further purification.

3.8. (*E*)-4′-{3,5-Bis[(2,5-bis(hexyloxy)-4-(styrylphenyl))styrylphenyl]phenyl}-2,2′:6′,2″-terpyridine (**11**)

A solution of (*E*)-2,5-bis(hexyloxy)-4-(styrylphenyl)benzaldehyde (**5**) (1.0 g, 2.5 mmol) and 4′-(3,5-bis(diethylphosphonomethyl)phenyl)-2,2′:6′,2″-terpyridine (**2**) (0.76 g, 1.25 mmol) was prepared in 10 ml of dry THF in an oven-dried, 50 ml round bottom flask. While the solution was cooled with an ice bath, potassium *tert*-butoxide (0.1 M in THF, 37.5 ml) was added dropwise via a syringe over a period of 0.5 h under an argon atmosphere. The reaction mixture was further stirred overnight at room temperature. After removing THF solvent on a rotary evaporator, the residues were purified on silica gel column (CH_2Cl_2: MeOH = 100:1) to give a yellow solid (0.5 g, 36.5%). ^{1}H NMR ($CDCl_3$, 300 MHz, δ ppm): 8.84 (s, 2H), 8.80 (d, $J = 4.8$ Hz, 2H), 8.74 (d, $J = 8.1$ Hz, 2H), 7.92 (s, 2H), 7.90 (m, 1H), 7.83 (s, 1H), 7.67 (s, 1H), 7.61 (s, 1H), 7.58 (s, 2H), 7.56 (s, 3H), 7.51 (s, 1H), 7.40 (m, 7H), 7.28 (d, $J = 5.7$ Hz, 4H), 7.22 (d, $J = 4.2$ Hz, 3H), 7.18(s, 2H), 7.16 (s, 1H), 4.13 (m, 8H), 1.93 (m, 8H), 1.60 (m, 16H), 0.96 (t, $J = 7.2$ Hz, 6H), 0.84 (t, $J = 7.2$ Hz, 6H). ^{13}C NMR ($CDCl_3$, 75 MHz, δ ppm): 156.52, 156.18, 151.37, 150.55, 149.37, 139.62, 139.29, 138.23, 137.14, 129.07, 129.02, 128.88, 127.65, 127.46, 127.22, 127.11, 127.05, 126.78, 125.79, 125.18, 124.75, 124.17, 124.11, 123.79, 121.68, 119.24, 119.15, 110.99, 110.40, 70.14, 69.89, 69.75, 69.46, 31.90, 31.83, 29.75, 29.65, 29.50, 26.18, 25.79, 22.86, 14.31. Anal. Calcd for $C_{77}H_{87}N_3O_4$: C, 82.68; H, 7.84; N, 3.76; O, 5.72. Found: C, 82.04; H, 7.87; N, 3.69; O, 6.19.

3.9. Synthesis of zinc complex **11**–Zn

To a stirred solution of zinc chloride (13 mg, 0.096 mmol) in EtOH (10 ml) was added dropwise a solution of **11** (80 mg, 0.072 mmol) in $CHCl_3$ (10 ml). After the addition was completed, the resulting mixture was heated to reflux for 5 h. The solution was cooled to room temperature and solvent was removed under reduced pressure over rotary evaporator. The residue was washed with EtOH/$CHCl_3$ (9/1) mixed solvent (10 ml) and then water (1 ml), 61 mg of yellow solid was obtained (68.0%). ^{1}H NMR ($CDCl_3$, 300 MHz, δ ppm): 8.98 (s, 2H), 8.18 (d, $J = 4.8$ Hz, 2H), 8.09 (m, 2H), 7.69 (m, 5H), 7.53 (m, 6H), 7.39 (m, 8H), 7.27 (m, 4H), 7.18 (m, 6H), 4.11 (m, 8H), 1.92 (m, 8H), 1.59 (m, 16H), 0.91 (m, 12H). Anal. Calcd for $C_{77}H_{87}Cl_2N_3O_4Zn$: C, 73.70; H, 6.99; Cl, 5.65; N, 3.35; O, 5.10. Found: C, 72.12; H, 6.93; Cl, 6.93; N, 4.26; O, 5.20.

4. Conclusion

A terpyridine-functionalized poly[(*m*-phenylenevinylene)-*alt*-(*p*-phenylenevinylene)] (P*m*PV*p*PV) derivative **2b** has been synthesized by using the Wittig condensation. The fluorescent polymer was found to interact with various metal ions, with the fluorescence quenching in the order of $Cu^{2+} > Co^{2+} > Ni^{2+} > Hg^{2+} > Zn^{2+} > Cd^{2+}$. Greater fluorescence quenching from Cu^{2+} ion indicates its potential as chemosensor. In addition, the Cr^{3+}, Fe^{3+}, and Mn^{2+} ions did not quench the fluorescence. The results are in contrast with its isomeric polymer **1**, whose solution fluorescence in $CHCl_3$–MeOH is reported to be completely quenched by Fe^{3+}, Ni^{2+}, Cu^{2+}, Cr^{3+}, Mn^{2+}, and Co^{2+} [20]. The observation indicates that the presence of *meta*-phenylene linkage in P*m*PV*p*PV weakens the electronic connection between the chromophore and metal-chelation site, thereby attenuating the metal ion-induced fluorescence quenching to allow the observed selectivity. Using Stern–Volmer analysis, the fluorescence quenching process is shown to be contributed from a combination of static and dynamic processes. The nonlinear Stern–Volmer plot, observed from both polymer and model compound, is attributed to the metal chelation.

Zinc(II) chelation of **2b** exhibits rather weak fluorescence quenching, accompanied with the new emission band at a longer wavelength (~570 nm). The fluorescence signal of **2b** is notably (~30 times) more sensitive to Zn^{2+}-induced quenching than that of the model compound **11** (Figs. 8 and 9). With the aid of model compound, the new emission band is attributed to the formation of tpy:Zn^{2+} complex in the 1:1 ratio. The fluorescence of **11**–Zn reveals that nearly all tpy remain in the chelation state in the dilute solution (Fig. 12), since the signal from the free ligand **11** (at ~460 nm) is negligible. It can be assumed that the zinc-chelated polymer **2b**–Zn remains to be in the tightly bonded state once it is formed in the solution. Structural similarity at the tpy chelation site

in **2b** and **11** suggests the similar zinc-binding capability in both molecules. The magnified fluorescence quenching observed from **2b** leads us to believe that the exciton migration along the polymer chain remains to be an important factor in the fluorescence quenching process.

Acknowledgement

This work was supported by the ERC program of the National Science Foundation (Award Number EEC-9731680) and The University of Akron. We also wish to thank The National Science Foundation (CHE-9977144) for funds used to purchase the NMR instrument used in this work.

References

[1] Que EL, Domaille DW, Chang CJ. Chem Rev 2008;108:1517–49.
[2] US EPA. Fed Regist 1979;44:69464.
[3] Heavy metals in the environment: origin, interaction and remediation. Amsterdam: Elsevier; 2005.
[4] Fluorescent chemosensors for ion and molecule recognition. Washington, DC: American Chemical Society; 1992.
[5] Rurack K, Kollmannsberger M, Resch-Genger U, Daub J. J Am Chem Soc 2000;122:968–9.
[6] Tang XL, Peng XH, Dou W, Mao J, Zheng JR, Qin WW, et al. Org Lett 2008;10:3653–6.
[7] Maeda H, Tierney DL, Mariano PS, Banerjee M, Cho DW, Yoon UC. Tetrahedron 2008;64:5268–78.
[8] Silva APD, Gunaratne HQN, Gunnlaugsson T, Huxley AJM, McCoy CP, Rademacher JT, et al. Chem Rev 1997;97:1515–66.
[9] Sung K, Fu H-K, Hong S-H. J Fluoresc 2008;17:383–9.
[10] Hofmeier H, Schubert US. Chem Soc Rev 2004;33:373–99.
[11] Andres PR, Schubert U. Adv Mater 2004;16:1043–68.
[12] Yu S-C, Kwok C-H, Chan W-K, Che C-M. Adv Mater 2003;15:1643–7.
[13] Chen YY, Tao YT, Lin HC. Macromolecules 2006;39:8559–66.
[14] Chiper M, Meier MAR, Wouters D, Hoeppener S, Fustin CA, Gohy JF, et al. Macromolecules 2008;41:2771–7.
[15] Hwang S-H, Wang P, Moorefield CN, Godínez LA, Manríquez J, Bustos E, et al. Chem Commun 2005:4672–4.
[16] Gratzel M. Inorg Chem 2005;44:6841–51.
[17] Thomas SW, Joly GD, Swager TM. Chem Rev 2007;107:1339–86.
[18] Zhang Y, Murphy CB, Jones Jr WE. Macromolecules 2002;35:630–6.
[19] Kraft A, Grimsdale AC, Holmes AB. Angew Chem Int Ed 1998;37:402–28.
[20] Kimura M, Horai T, Hanabusa K, Shirai H. Adv Mater 1998;10:459–62.
[21] Pang Y, Li J, Hu B, Karasz FE. Macromolecules 1999;32:3946–50.
[22] Liao L, Pang Y, Ding L, Karasz FE. Macromolecules 2002;35:3819–24.
[23] Dumur F, Mayer CR, Dumas E, Miomandre F, Frigoli M, Sécheresse F. Org Lett 2008;10:321–4.
[24] Lawrence NJ. In: Williams JMJ, editor. Preparation of alkenes: a practical approach. Oxford: Oxford University Press; 1996. p. 19–58.
[25] Gispert JR. Coordination chemistry. Weinheim: Wiley-VCH; 2008.
[26] Bertrand H, Monchau D, De Cia A, Guillo R, Mergn J-L, Teulade-Ficho M-P. Org Biomol Chem 2007;5:2555–9.
[27] Nielsen P, Toftlund H, Boas J, Pilbrow JR, Moubaraki B, Murray K, et al. Inorg Chim Acta 2008;361:3453–61.
[28] Demas JN, Crosby GA. J Phys Chem 1971;75:991–1024.
[29] Dobrawa R, Lysetska M, Ballester P, Grune M, Wurthner F. Macromolecules 2005;38:1315–25.
[30] (a) Valeur B. Effects of intermolecular photophysical process on fluorescence emission. In: Molecular fluorescence. Weinheim: Wiley-VCH; 2001;
(b) Blatt E, Mau AW-H, Sasse WHF, Sawyer WH. Aust J Chem 1988;41:127–31.
[31] Murphy CB, Zhang Y, Troxler T, Ferry V, Martin JJ, Jones WE. J Phys Chem B 2004;108:1537–43.
[32] Chu Q, Pang Y. J Polym Sci Part A Polym Chem 2006;44:2338–45.
[33] Lakowicz JR. Principles of fluorescence spectroscopy. New York: Kluwer Academic; 1999. p. 51–5.
[34] Witiak DT, Loper JT, Ananthan S, Almerico AM, Verhoef VL, Flippi JA. J Med Chem 1989;32(7):1636–42.